Eur. Phys. J. D **1**, 15–28 (1998)

THE EUROPEAN PHYSICAL JOURNAL D

Quantum Zenon effects in composite systems

R. Wawer, M. Keller, A. Liebman, and G. Mahler[a]

Institut für Theoretische Physik, Universität Stuttgart, Pfaffenwaldring 57, 70550 Stuttgart, Germany

Received: 15 April 1997 / Revised: 25 June 1997 / Accepted: 18 October 1997

Abstract. Quantum Zenon effects are discussed in terms of a specific class of quantum trajectories, which are conditioned by continuous, mutually exclusive measurement signals. Such a conditioning is not restricted to simple systems but can be generalized to composite networks. In any case, the characteristic features of these trajectories tend to be washed out in the ensemble limit and thus require single system analysis. Only on a sufficiently small time-scale and for a coherent initial state, also the ensemble exhibits some Zenon effect. In this case, ironically, actual measurements are not required: a closed single composite system can emulate this behavior. Such a kind of quantum parallelism underlies also recent proposals for quantum computation.

PACS. 42.50.Lc Quantum fluctuations, quantum noise, and quantum jumps – 42.25.Kb Coherence

1 Introduction

How can a physical property change, if its value is to exist (sharply) at any instant of time? The Greek philosopher Zenon came to the conclusion that the concepts of a *well-specified property* and of *change* were incompatible. For continuous evolution a modern way out of this apparent paradox is based on the concept of the derivative. In quantum physics, however, we often encounter observables with discrete spectra [1], for which this remedy does not work. How can these change, then?

Quantum Zenon effects are generally associated with scenarios, in which attempts to "observe motion" (in a discrete state space) tend to suppress it.

Time-resolved observations in a discrete state space can be based on binary decisions, which must be substantiated by a measurement model (logic of inference). From this information point of view quantum Zenon effects would show up as the tendency for decisions to confirm previous ones: this behavior defines a class of "conditioned dynamics".

Originally [2,3], a "clocked Zenon effect" has been discussed in the context of idealized measurement projections performed at discrete instants of time. In the simplest approximation, this constitutes an interrupted unitary motion. It was then predicted that with the number of state-selective measurements, r, going to infinity, this very state should "freeze-in " completely. This phenomenon has therefore alternatively been termed "watchdog effect" [4]. It is in accord with the standard requirement that the "immediate" repetition of a measurement should reproduce the previous result [5]. From this latter point of view the Zenon effect could hardly be called paradoxical, even though it still appears to be counterintuitive.

Such a clocked Zenon effect has recently been realized experimentally [6] based on a certain number of measurement pulses of (necessarily) finite duration. The system considered was an *ensemble* of effective 3-level systems (laser-cooled ions in a Penning trap), all being prepared in the same initial state $|1\rangle$ and exposed to a rf-π-pulse resulting in a transition to state $|2\rangle$, if unperturbed. During this evolution the dissipative transition $|1\rangle \rightarrow |3\rangle$ could be addressed by measurement pulses of length short compared with the π-pulse length. The experiment showed that the percentage of ions on a trajectory reaching state $|2\rangle$ at the end of the nominal π-pulse, indeed, decreased with the number of such measurements.

To the best of our knowledge, no further attempt has been made to attack the Zenon effect experimentally [7], despite ongoing theoretical discussions [8–14]. What does this imply? Should Zenon effects be considered so ubiquitous that they do not deserve special attention, let alone carefully designed scenarios which artificially timed measurements? Or are they so "exotic" that they are of no concern to everyday quantum experiments? In any case, are quantum Zenon effects understood well enough to put them aside?

The fact that damping (associated with any measurement) modifies the dynamics should be no surprise, indeed. Zenon effects could be interpreted to mean: (i) freezing into measurement states, (ii) suppression of superpositions, (iii) correlation with information retrieval. We suggest to discuss these potential characteristics, even though too narrow as they stand, in the context of quantum trajectories: we are thus looking for a class of "Zenon-trajectories".

[a] e-mail: mahler@theo.physik.uni-stuttgart.de

As will be shown in the following, Zenon-trajectories turn out to be quite common but require parameter windows constituting a specific "logic of inference": it is this logic which guarantees distinguishability of (in the simpliest case) two different measurement outcomes (signal trains, not single events), which, in turn, are then correlated with the respective quantum trajectory being constrained to two different regions in Hilbert-space. (The separation disappears as the damping rate goes to zero; this feature discriminates Zenon effects from simple stationary state subspaces.)

In general, this separation is washed out in an ensemble as each individual ensemble member continues to jump randomly between the two Hilbert-space regions (leading to ensemble-averaged state parameters). The asymptotic attractor state of the ensemble, to be sure, has nothing to do with the Zenon-effect proper. Only at small timescales (in the experiment cited 1/2 Rabi-cycle) and with ensemble members all starting in the same initial state does the Zenon effect remain observable: pulsed measurements, though allowing a well-defined decomposition into unitary motion and projections, are by no means essential.

However, if ensemble dynamics suffices [15], any information related to individual concrete measurement results should be irrelevant. Indeed, such an ensemble behavior can be emulated by one object-subsystem (out of a closed N-two-level network) under the influence of the other $N-1$ subsystems, sequentially coupled to the object system one at a time. This is reminiscent of the Wigner-Weisskopf theory, in which a single subsystem, coupled to an (infinite) set of oscillators, say, is shown to emulate ensemble decay.

It will be pointed out that the deterministic trajectory of the object system can be seen as an ensemble-mixture of Zenon-trajectories under $N-1$ pulsed measurements. This behavior is a simple example of "quantum parallelism" (one single system emulating an ensemble), a prominent feature of quantum computation. Even though there is no "watchdog" in this case, we do not see any reason to put this example outside the Zenon-effect proper [8–10].

This paper is organized as follows: in Section 2 we introduce the concept of cluster-operators underlying our model- and state-descriptions as well as the concept of quantum trajectories, Section 3 deals with special "Zenon-trajectories" of open networks, Section 4, finally is concerned with closed but explicitly time-dependent networks, allowing to generate "mixtures" of conditioned subsystem-trajectories ("quantum parallelism"). The results are summarized in Section 5.

2 Network model

2.1 Cluster operators

Consider a network composed of $N = 3$ subsystems ($\mu = 1,\ 2,\ 3$) with $n = 2$ local states each, $|p(\mu)\rangle$, $p = 1,\ 2$. Product states of these form a standard basis for the total network. It is convenient to think of operators acting on the network-states in terms of "cluster-operators", which operate on $m \leq N$ subsystems, while leaving the others unchanged. The no-change-operator is the unit-operator, $\hat{\lambda}_0(\mu) = \hat{1}(\mu)$; as the remaining $n^2 - 1 = 3$ orthogonal local operators we take the (traceless) generators of a $SU(2)$-algebra (see Append. A): $\hat{\lambda}_j(\mu)$, $j = 1, 2, 3$. The local basis states $|p(\mu)\rangle$ are assumed to coincide with the eigenstates of $\hat{\lambda}_3(\mu)$: eigenvalue -1 corresponds to state $|1(\mu)\rangle$, eigenvalue $+1$ to the excited state $|2(\mu)\rangle$. With the convention that we do not write the unit operators explicitly, the $m = 1$-cluster-operators are simply given by the $\hat{\lambda}_j(\mu)$, $j = 1, 2, 3$. The cluster operators for $m = 2, 3$ are (*cf.* [16,17])

$$\begin{aligned} \hat{K}_{ij}(\mu\nu) &= \hat{\lambda}_i(\mu)\hat{\lambda}_j(\nu) \\ \hat{K}_{ijk}(123) &= \hat{\lambda}_i(1)\hat{\lambda}_j(2)\hat{\lambda}_k(3). \end{aligned} \tag{1}$$

Then, any operator $\hat{A}$ can be represented as (summation over repeated indices)

$$\hat{A} = \frac{1}{8}\Bigg[A_0\hat{1} + \sum_{\mu} A_i^{\mu}\hat{\lambda}_i(\mu) + \sum_{\mu<\nu} A_{ij}^{\mu\nu}\hat{K}_{ij}(\mu\nu) + A_{ijk}^{123}\hat{K}_{ijk}(123)\Bigg] \tag{2}$$

with $A_0 = \mathrm{Tr}\ \{\hat{A}\,\hat{1}\}$, $A_i^{\mu} = \mathrm{Tr}\ \{\hat{A}\,\hat{\lambda}_i(\mu)\}$, $A_{ij}^{\mu\nu} = \mathrm{Tr}\ \{\hat{A}\,\hat{K}_{ij}(\mu\nu)\}$, *etc.* This hierarchy of parameters uniquely specifies $\hat{A}$.

2.2 Hamilton-parameters

When this representation is applied to the Hamilton operator $\hat{H} = \sum_{\mu}\hat{H}(\mu) + \sum_{\mu<\nu}\hat{H}(\mu,\nu)$, one finds the hierarchy of parameters

$$\begin{aligned} H_0 &= \mathrm{Tr}\ \{\hat{H}\hat{\lambda}_0\} \\ H_i^{\mu} &= \mathrm{Tr}\ \{\hat{H}\hat{\lambda}_i(\mu)\} \\ H_{ij}^{\mu\nu} &= \mathrm{Tr}\ \{\hat{H}\hat{K}_{ij}(\mu,\nu)\}. \end{aligned} \tag{3}$$

For a network of three driven 2-level systems in rotating-wave-approximation (δ=detuning, g=field intensity),

$$\hat{H}(\mu) = \frac{1}{2}\hbar\delta_{21}^{\mu}(\hat{P}_{22}(\mu) - \hat{P}_{11}(\mu)) + \frac{1}{2}\hbar g_{21}^{\mu}(\hat{P}_{12}(\mu) + \hat{P}_{21}(\mu)) \tag{4}$$

and for an Ising-spin-type interaction

$$\hat{H}(\mu\nu) = -\frac{1}{2}\hbar C_{\mathrm{R}}^{\mu\nu}(\hat{P}_{22}(\mu) - \hat{P}_{11}(\mu))(\hat{P}_{22}(\nu) - \hat{P}_{11}(\nu)) \tag{5}$$

the set of non-zero parameters reduces to

$$H_1^{\mu} = 4\hbar g_{21}^{\mu}$$

$$H_3^{\mu} = 4\hbar\delta_{21}^{\mu} \tag{6}$$

$$H_{33}^{\mu\nu} = -4\hbar C_{\mathrm{R}}^{\mu\nu}. \tag{7}$$

2.3 State-parameters

In the same way the density operator can be represented by the expectation values

$$\begin{aligned}\lambda_0 &= \mathrm{Tr}\,\{\hat{\rho}\hat{\lambda}_0\} = 1\\ \lambda_i^\mu &= \mathrm{Tr}\,\{\hat{\rho}\hat{\lambda}_i(\mu)\} = \left\langle \hat{\lambda}_i(\mu)\right\rangle\\ K_{ij}^{\mu\nu} &= \mathrm{Tr}\,\{\hat{\rho}\hat{K}_{ij}(\mu,\nu)\}\\ K_{ijk}^{123} &= \mathrm{Tr}\,\{\hat{\rho}\hat{K}_{ijk}(1,2,3)\}\,. \end{aligned} \tag{8}$$

In general, all cluster-operatos (here up to $m = 3$) contribute. The real-valued parameter-set

$$\Gamma = \{\lambda_i^\mu, K_{ij}^{\mu\nu}, ...\} \tag{9}$$

uniquely specifies the state of the network. (Expectation values for mixed states will be overlined, $\overline{\lambda_i^\mu}$ *etc.*) For later reference we also introduce the "covariances" (correlation tensors proper [16]),

$$\begin{aligned} M_{ij}^{\mu\nu} &= \left\langle (\hat{\lambda}_i(\mu) - \lambda_i^\mu)(\hat{\lambda}_j(\nu) - \lambda_j^\nu)\right\rangle\\ &= K_{ij}^{\mu\nu} - \lambda_i(\mu)\lambda_j(\nu) \end{aligned} \tag{10}$$

$$M_{ijk}^{123} = \left\langle (\hat{\lambda}_i(1) - \lambda_i^1)(\hat{\lambda}_j(2) - \lambda_j^2)(\hat{\lambda}_k(3) - \lambda_k^3)\right\rangle. \tag{11}$$

Note that $M_{ij}^{\mu\nu}$, which includes up to $m = 2$-cluster-operators, and M_{ijk}^{123}, which includes up to $m = 3$, are zero if and only if $\hat{\rho}$ is a product state (*i.e.* if not "entangled"). These terms thus allow to test entanglement. Convenient measures are [16]

$$\beta^{\mu\nu} = \frac{1}{3}\sum_{ij} M_{ij}^{\mu\nu} M_{ij}^{\mu\nu} \le 1 \tag{12}$$

$$\beta^{123} = \frac{1}{4}\sum_{ijk} M_{ijk}^{123} M_{ijk}^{123} \le 1. \tag{13}$$

They allow to compress the otherwise cumbersome entanglement data to a few positive definite numbers, which, furthermore, are invariant under any local unitary transformation [16].

2.4 Dynamics

The master equation of the density operator is given by

$$\frac{\mathrm{d}}{\mathrm{d}t}\hat{\rho} = \hat{L}\hat{\rho} = \hat{L}^{(0)}\hat{\rho} + \hat{L}^{(H)}\hat{\rho} + \hat{L}^{(P)}\hat{\rho}\,, \tag{14}$$

where

$$\hat{L}^{(0)}\hat{\rho} = \frac{1}{I\hbar}[\hat{H},\,\hat{\rho}] \tag{15}$$

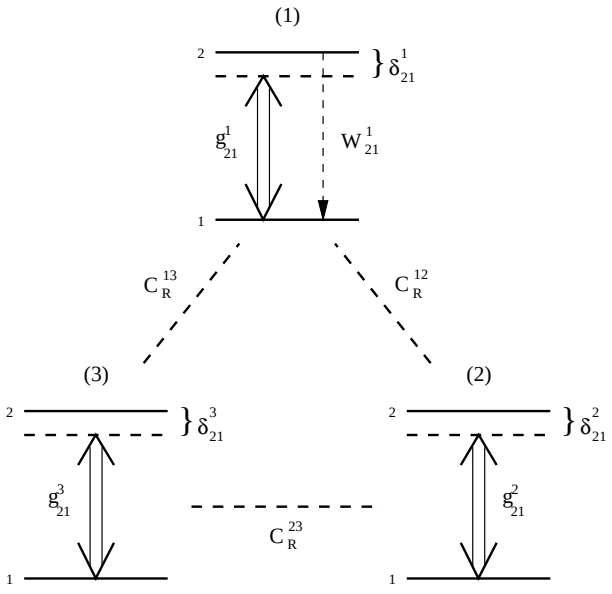

Fig. 1. Networks of $N = 3$ two-level systems as considered in this paper. g_{21}^μ are local coupling strengths to coherent light fields, δ_{21}^μ is the detuning, $C_{\mathrm{R}}^{\mu\nu}$ describe inter-node coupling, W_{12}^1 is the transition rate for the single damping channel in subsystem 1.

is the unitary part. Here we will restrict ourselves to a single dissipative channel in subsystem $\mu = 1$, (*cf.* Fig. 1), for which

$$\hat{L}^{(H)}\hat{\rho} = -\frac{1}{2}W_{12}^1\left[\hat{\rho}\,\hat{P}_{12}^+(1)\hat{P}_{12}(1) + \hat{P}_{12}^+(1)\hat{P}_{12}(1)\,\hat{\rho}\right] \tag{16}$$

$$\hat{L}^{(P)}\hat{\rho} = W_{12}^1\hat{P}_{12}(1)\,\hat{\rho}\,\hat{P}_{12}^+(1). \tag{17}$$

W_{12}^1 is the corresponding transition rate from state $|2\rangle$ to $|1\rangle$. The respective $SU(2)$-representation of $\hat{L}\hat{\rho}$ is given in Appendix B. In general, under the influence of equation (14), $\hat{\rho}$ does not remain pure, which is interpreted as an ensemble effect: Stochastic unraveling [18] maintains that each individual ensemble member follows a pure-state trajectory, which is generated by the truncated continuous evolution [16,18]

$$\hat{\rho}(t + \mathrm{d}t) = \hat{\rho}(t) + \left(\hat{L}^{(0)}\hat{\rho} + \hat{L}^{(H)}\hat{\rho}\right)\mathrm{d}t. \tag{18}$$

interrupted by occasional projections by $\hat{L}^{(P)}$,

$$\hat{\rho}'(t + \mathrm{d}t) = \begin{cases} \dfrac{\hat{\rho}(t + \mathrm{d}t)}{\lambda_0(t + \mathrm{d}t)} & z \ge R^1 \\ \text{for} & \\ \dfrac{\hat{L}^{(P)}\hat{\rho}(t + \mathrm{d}t)}{\mathrm{Tr}\,\{\hat{L}^{(P)}\hat{\rho}(t + \mathrm{d}t)\}} & z < R^1 \end{cases} \tag{19}$$

where

$$\lambda_0(t + \mathrm{d}t) = \mathrm{Tr}\,\{\hat{\rho}(t + \mathrm{d}t)\} = 1 - R^1 \tag{20}$$

and z is a random number, $0 \le z \le 1$. Sampling over many such pure-state trajectories we find a joint distribution function $f(\Gamma, t)$, where Γ has been introduced in

equation (9). Defining $\overline{\lambda_i^\mu}(t) = \int \lambda_i^\mu f(\Gamma,t)\mathrm{d}\Gamma$ *etc.*, the set $\overline{\Gamma}(t) = \{\overline{\lambda_i^\mu}(t), \overline{K_{ij}^{\mu\nu}}(t), \dots\}$ is equivalent to the ensemble solution of the master equation. $f(\Gamma,t)$ specifies a pure-state decomposition of the ensemble density matrix.

2.5 Parameter window for conditioning

Conditioning is a central feature required to (logically) infer from the behavior of one subsystem the state of another subsystem. In the simpliest case we have an interacting pair of 2-level systems $\mu = 2$ (conditioning) and $\mu = 1$ (conditioned system) without damping (see Fig. 1, node 3 is not needed here). We restrict ourselves to pure states for which the equations of motion read (*cf.* Append. B):

$$\dot\lambda_i^1 = \Omega_{il}^{11}\lambda_l^1 + \frac{1}{2}Q_{iml}^{112}(M_{ml}^{12} + \lambda_m^1\lambda_l^2) \tag{21}$$

$$\dot\lambda_j^2 = \Omega_{jl}^{22}\lambda_l^2 + \frac{1}{2}Q_{jml}^{221}(M_{lm}^{12} + \lambda_m^1\lambda_l^2). \tag{22}$$

The correlation proper (see Eq. (10)) is controlled by

$$\dot M_{ij}^{12} = X_{ij} + (\Omega_{il}^{11} - \frac{1}{2}Q_{ilj}^{112})M_{lj}^{12} + (\Omega_{jl}^{22} - \frac{1}{2}Q_{jli}^{221})M_{il}^{12} \tag{23}$$

with

$$X_{ij} = \lambda_l^1(Q_{ilj}^{112} - Q_{ilm}^{112}\lambda_m^2\lambda_j^2) + \lambda_m^2(Q_{jmi}^{221} - Q_{jml}^{221}\lambda_l^1\lambda_i^1). \tag{24}$$

For the present Hamilton model (*cf.* Eqs. (B.6, B.9)), the only non-zero matrix elements are $\Omega_{12}^{\mu\mu} = -\delta_{21}^\mu, \Omega_{23}^{\mu\mu} = -g_{21}^\mu$, $Q_{231}^{212} = -Q_{132}^{212} = 2C_{\mathrm{R}}^{12}$ and $Q_{123}^{112} = -Q_{213}^{112} = 2C_{\mathrm{R}}^{12}$. Thus equations (21, 22) reduce to

$$\begin{aligned}
\dot\lambda_1^1 &= -\delta_{\mathrm{eff}}^1(t)\lambda_2^1 + C_{\mathrm{R}}^{12}M_{23}^{12}\\
\dot\lambda_2^1 &= \delta_{\mathrm{eff}}^1(t)\lambda_1^1 - g_{21}^1\lambda_3^1 - C_{\mathrm{R}}^{12}M_{13}^{12}\\
\dot\lambda_3^1 &= g_{21}^1\lambda_2^1\\
\dot\lambda_1^2 &= -\delta_{\mathrm{eff}}^2(t)\lambda_2^2 + C_{\mathrm{R}}^{12}M_{32}^{12}\\
\dot\lambda_2^2 &= \delta_{\mathrm{eff}}^2(t)\lambda_1^2 - g_{21}^2\lambda_3^2 - C_{\mathrm{R}}^{12}M_{31}^{12}\\
\dot\lambda_3^2 &= g_{21}^2\lambda_2^2
\end{aligned} \tag{25}$$

where we have introduced the state-dependent effective detuning parameters

$$\begin{aligned}
\delta_{\mathrm{eff}}^1(t) &= \delta_{21}^1 - C_{\mathrm{R}}^{12}\lambda_3^2(t)\\
\delta_{\mathrm{eff}}^2(t) &= \delta_{21}^2 - C_{\mathrm{R}}^{12}\lambda_3^1(t).
\end{aligned} \tag{26}$$

The set of equations is closed, if $M_{ik}^{12} = 0$. This is the case if we start with a product state and require $X_{ij} = 0$ (see Eq. (24)). With the above parameters Q, this condition is fulfilled, if either $\lambda_j^1 = \lambda_j^2 = 0, j = 1,2,3$, or $\lambda_3^1 = \pm 1$, or $\lambda_3^2 = \pm 1$.

Now, $\lambda_3^2 = \pm 1$, (*i.e.* $\lambda_1^2 = \lambda_2^2 = 0$) also solves the Bloch equations for node 2 (the control), provided g_{21}^2 is zero. Then $\delta_{\mathrm{eff}}^1 = \delta_{21}^1 \pm C_{\mathrm{R}}^{12}$ is constant and the respective Bloch equations for $\mu = 1$ reduce to

$$\begin{aligned}
\dot\lambda_1^1 &= -\delta_{\mathrm{eff}}^1\lambda_2^1\\
\dot\lambda_2^1 &= \delta_{\mathrm{eff}}^1\lambda_1^1 - g_{21}^1\lambda_3^1\\
\dot\lambda_3^1 &= g_{21}^1\lambda_2^1.
\end{aligned} \tag{27}$$

Under the no-correlation condition as specified above the interaction is seen to act as a state-dependent detuning: choosing for $\lambda_3^2 = -1$ (*i.e.* system 2 in state $|1\rangle$) an external driving field with $\delta_{21}^1 = -C_{\mathrm{R}}^{12}$, the solution is the resonant Rabi-oscillation

$$\lambda^1(t) = \left(0, \sin\left[g_{21}^1(t-t_0)\right], -\cos\left[g_{21}^1(t-t_0)\right]\right). \tag{28}$$

With the same driving field, but $\lambda_3^2 = 1$ (*i.e.* system 2 in state $|2\rangle$), the effective detuning is $\delta_{\mathrm{eff}}^1 = -2C_{\mathrm{R}}^{12}$ implying the solution

$$\begin{aligned}
\lambda_1^1 &= \frac{\delta_{\mathrm{eff}}^1 g_{21}^1}{(\Omega_{\mathrm{R}}^1)^2}(\cos\Omega_{\mathrm{R}}^1 t - 1)\\
\lambda_2^1 &= \frac{g_{21}^1}{\Omega_{\mathrm{R}}^2}\sin\Omega_{\mathrm{R}}^1 t\\
\lambda_3^1 &= -1 - \frac{(g_{21}^1)^2}{(\Omega_{\mathrm{R}}^1)^2}(\cos\Omega_{\mathrm{R}}^1 t - 1)
\end{aligned} \tag{29}$$

where

$$(\Omega_{\mathrm{R}}^1)^2 = (\delta_{\mathrm{eff}}^1)^2 + (g_{21}^1)^2 \tag{30}$$

is the respective Rabi-frequency. Under the "selectivity condition"

$$|\delta_{21}^1| = 2|C_{\mathrm{R}}^{12}| \gg g_{21}^1 \tag{31}$$

the controlled system's response is virtually zero. The eigenstates of system 2 thus condition the path of system 1, without back-action.

2.6 Logic of inference

When combined with measurement (information retrieval), conditioning defines a "logic of inference". For this to work, however, one has to go from the ensemble- to the single-system-level.

To illustrate the difference, we consider a test system, node 1 ($g_{21}^1 \neq 0$, $\delta_{21}^1 = -C_{\mathrm{R}}^{12}$), in contact with an object node 2. C_{R}^{12} is supposed to fulfill the selectivity condition, system 2 is not driven, $g_{21}^2 = 0$. The test system has a local damping channel W_{12}^1, generating incoherent transitions from its excited state $|2\rangle$ to the ground state $|1\rangle$. The equations of motion for the respective Bloch-vectors read (*cf.* Eqs. (25, and B.14, B.15))

$$\begin{aligned}
\dot{\bar\lambda}_1^1 &= -\delta_{\mathrm{eff}}^1\bar\lambda_2^1 + C_{\mathrm{R}}^{12}\bar M_{23}^{12} - \frac{1}{2}W_{12}^1\bar\lambda_1^1\\
\dot{\bar\lambda}_2^1 &= \delta_{\mathrm{eff}}^1\bar\lambda_1^1 - g_{21}^1\bar\lambda_3^1 - C_{\mathrm{R}}^{12}\bar M_{13}^{12} - \frac{1}{2}W_{12}^1\bar\lambda_2^1\\
\dot{\bar\lambda}_3^1 &= g_{21}^1\bar\lambda_2^1 - W_{12}^1\bar\lambda_3^1 - W_{12}^1
\end{aligned} \tag{32}$$

$$\dot{\bar{\lambda}}_1^2 = -\delta_{21}^2\bar{\lambda}_2^2 + C_{\rm R}^{12}\bar{M}_{32}^{12} + C_{\rm R}^{12}\bar{\lambda}_2^2\bar{\lambda}_3^1$$
$$\dot{\bar{\lambda}}_2^2 = \delta_{21}^2\bar{\lambda}_1^2 - C_{\rm R}^{12}\bar{M}_{31}^{12} - C_{\rm R}^{12}\bar{\lambda}_1^2\bar{\lambda}_3^1$$
$$\dot{\bar{\lambda}}_3^2 = 0 \qquad (33)$$

where $\delta_{\rm eff}^1 = -C_{\rm R}^{12}(1+\bar{\lambda}_3^2) = \text{constant}$. (The overlines indicate ensemble averages.) With $\bar{M}_{jk}^{12} \to 0$, due to damping, the stationary ensemble solution is found to be $\bar{\lambda}_1^2 = \bar{\lambda}_2^2 = 0$, $\bar{\lambda}_3^2 = \bar{\lambda}_3^2(t=0)$, while the driven test system 1 ends up in the well-known stationary state of the damped Bloch equations. This is an ensemble measurement of $\hat{\lambda}_3(2)$.

In the stochastic simulation for a single quantum network, λ_3^2 is no longer constant: after an individual jump in the test system the Bloch-vector of subsystem 2 is updated according to (*cf.* [16])

$$(\lambda_j^2)' = \lambda_j^2 + \frac{1}{2P_2^1}M_{j3}^{21}$$
$$(M_{jk}^{21})' = 0. \qquad (34)$$

P_2^1 is the probability to find test system 1 in state $|2\rangle$. In general, after such a jump entanglement builds up again (see Sect. 4.1). There are, however, two attractor states, $\lambda_3^2 = \mp 1$, in which case M_{jk}^{12} remains zero. These are reached with high probability provided the driving pulse on test system 1 is long enough. This underlines the fact that measurement pulses necessarily consume a finite period of time, they cannot be instantaneous (incomplete measurements may have various origins [19]). This finite duration is a principle limitation of any measurement and invalidates the concept of "instantaneous projection" needed to let the "number of measurements" within finite time to go to infinity: this asymptotic result (and only this!) would lead to a complete freezing of the measurement state, as discussed in [2,6].

A numerical simulation is shown in Figure 2. With the chosen resonance condition the asymptotic projection of system 2 into state $|1\rangle$ ($\lambda_3^2 = -1$) is signaled by an intensive sequence of luminescence photons emitted by the test system. Projection into $|2\rangle$ would let the luminescence virtually die out. Both asymptotic states are stable. The outcome of any individual trajectory is unpredictable. Note that the signal to "continuously" monitor the type of state is not a single detection event but rather a continuous trace of photons/no photons, respectively. Averaging over many such trajectories leads back to the ensemble result with averaged luminescence (without "decision" or switching).

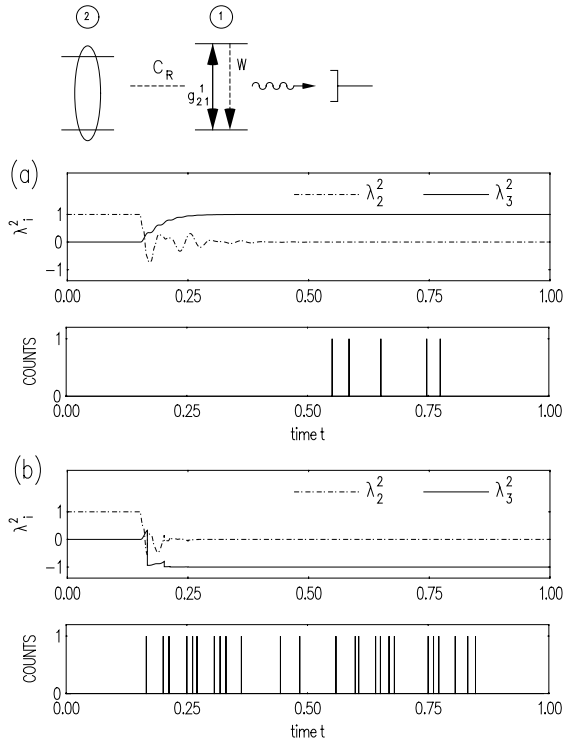

Fig. 2. Measurement projection: Recorded decisions for network (N=2). System 2 is prepared in the superposition state ($\lambda_2^2 = 1$), which conditions subsystem 1. Time in arbitrary units τ. ($W_{12}^1 = 75$, $g_{21}^1 = 150$, $C_{\rm R}^{12} = -\delta_{21}^1 = -\delta_{21}^2 = 500$, all in units τ^{-1}. The same units are used in the subsequent figures.) (a) asymptotic state $\lambda_3^2 = -1$, (b) asymptotic state $\lambda_3^2 = +1$. The measurement pulse, g_{21}^1, is switched on at time 0.15 and switched off at 0.85.

3 Open networks: continuous measurements

3.1 Conditioned trajectories

In the stochastic simulation the single dissipative channel (single "output") in subsystem 1, implies jumps related to the emission of photons and thus generates a measurement record (*cf.* Fig. 2). On a larger time-scale and within appropriate parameter windows one may be able to distinguish "dark" and "light" periods by which the trajectories should be conditioned. Contrary to the simple von Neumann projection, for continuous measurement of this type the symmetry between the two measurement outcomes is broken by the fact that one is associated with the emission of photons ("luminescence state"), the other is not ("no-luminescence state"). While the "capture" in the light emitting subspace can be understood as the result of continuous reset jumps associated with photon emission, this intuitive picture fails for the no-luminescence state.

The salient features, however, can be understood already from studying the simpliest network, one driven and damped 2-level system. (In this case, to be sure, the non-luminescence state is not stable).

Let us first recall that the non-unitary dynamics conditioned by seeing no jump (no luminescence) can be written as (*cf.* Eq. (18) and Append. B)

$$\hat{\rho}(t+{\rm d}t) = \hat{\rho}(t) - \frac{I}{\hbar}[\hat{H}_{\rm eff}\hat{\rho} - \hat{\rho}\hat{H}_{\rm eff}^{+}]{\rm d}t \qquad (35)$$

where for a two-level system with one damping channel W_{12}

$$\hat{H}_{\rm eff} = \hat{H} - \frac{I\hbar}{2}W_{12}\hat{P}_{22}. \qquad (36)$$

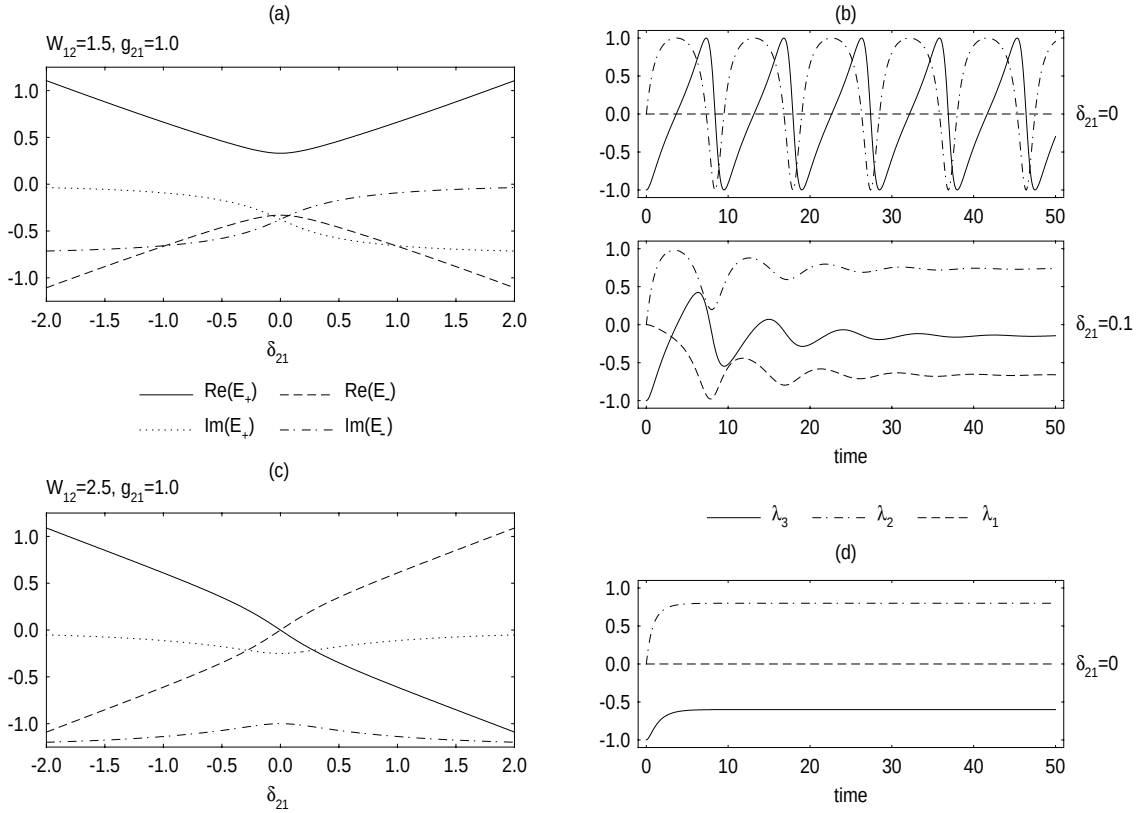

Fig. 3. Complex dressed states in $SU(2)$, (a) eigenvalues for weak damping, $W_{12} = 1.5$; $g_{21} = 1.0$, (b) corresponding dynamics of Bloch-vector, $\delta_{21} = 0$, $\delta_{21} = 0.1$, respectively, (c) eigenvalues for strong damping, $W_{12} = 2.5$; $g_{21} = 1.0$, (d) corresponding dynamics of Bloch-vector, $\delta_{21} = 0$.

The matrix representation of the non-Hermitian $\hat{H}_{\rm eff}$ in the eigenbasis of $\hat{\lambda}_3$ thus reads

$$\mathbf{H}_{\rm eff} = \frac{\hbar}{2}\begin{pmatrix} -\delta_{21} & g_{21} \\ g_{21} & \delta_{21} - IW_{12} \end{pmatrix}. \tag{37}$$

The right-hand eigenvalue equation

$$\hat{H}_{\rm eff}|{\rm e}_j\rangle = E_j|{\rm e}_j\rangle \tag{38}$$

has the complex eigenvalues given by

$$E_\pm = \pm\hbar(a_+ + Ia_-) - I\hbar\frac{W_{12}}{4} \tag{39}$$

and the (non-orthogonal) eigenvectors

$$\begin{aligned} |{\rm e}_+\rangle &= \frac{g_{21}}{2}\,|1\rangle + \left(\frac{\delta_{21}}{2} + E_+\right)|2\rangle \\ |{\rm e}_-\rangle &= -\left(\frac{\delta_{21}}{2} + E_+\right)|1\rangle + \frac{g_{21}}{2}\,|2\rangle \end{aligned} \tag{40}$$

where the abbreviations introduced are

$$\begin{aligned} a_\pm = \frac{S_\pm}{2}\Bigg[\frac{1}{2}\sqrt{\left((\Omega_{\rm R})^2 - \frac{(W_{12})^2}{4}\right)^2 + (W_{12})^2(\delta_{21})^2} \\ \pm\frac{1}{2}\left((\Omega_{\rm R})^2 - \frac{(W_{12})^2}{4}\right)\Bigg]^{1/2} \end{aligned} \tag{41}$$

with $\Omega_{\rm R}$ denoting the Rabi-frequency (*cf.* Eq. (30)). The $S_\pm$ control the signs: S_+ is negative for $2g_{21} < W_{12}$ and $\delta_{21} > 0$, S_- is negative for $2g_{21} \geq W_{12}$ and $\delta_{21} > 0$, while both are positive otherwise. The corresponding left-side eigenvalue equation is

$$\langle\tilde{\rm e}_j|\hat{H}_{\rm eff} = \langle\tilde{\rm e}_j|E_j. \tag{42}$$

These eigenvalues can be normalized to give

$$\langle\tilde{\rm e}_i|{\rm e}_j\rangle = \delta_{ij} \tag{43}$$

and thus allow the expansion

$$|\psi\rangle = \sum_j |{\rm e}_j\rangle\langle\tilde{\rm e}_j|\psi\rangle. \tag{44}$$

Complex dressed states have been discussed previously, though within a different context (see [20–22]). Numerical results for the real and the imaginary part of the two eigenvalues $E_\pm$ are shown in Figure 3a for the weak damping case ($W_{12} < 2g_{21}$). Figure 3b shows the subensemble dynamics (initial state = ground state $|1\rangle$) based on equation (35) in terms of the Bloch-vector. For zero detuning the motion remains periodic: this can easily be understood from the fact that the real parts of the two eigenvalues are different, while the imaginary parts are identical: expressing the prepared initial state as a certain superposition of

the two complex eigenstates implies that both decay with the same decay constant so that their weight after renormalization remains constant. This evolution is (logically) reversible [23].

For $\delta_{21} \neq 0$ the imaginary parts of the two eigenvalues are different so that only one solution (with the smaller imaginary part) survives: a relaxation into a unique attractor state results, reversibility is eventually lost, even though the trajectory is entirely deterministic (this typical case has been overlooked in [23]).

In the strong damping limit $W_{12} > 2g_{21}$ (Fig. 3c) the imaginary parts are different for any detuning so that the only type of dynamics is (overdamped) relaxation into a stationary state (Fig. 3d). In either case the attractor state is a coherent state which would approach $|1\rangle$ for $W_{12} \gg g_{21}$ only. This latter state is also the state stabilized by frequent projections (related with photon emission). The state in the "dark period" thus asymptotically approaches the state in the "light period", the stable fix point.

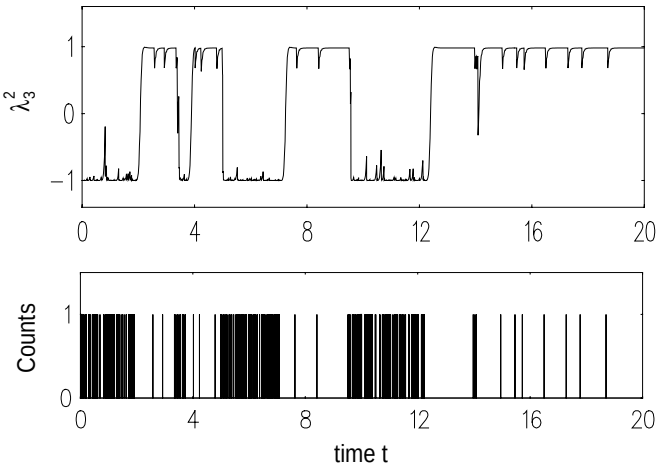

Fig. 4. Zenon effect in a single pair of coupled two-level subsystems. ($W_{12}^1 = 70$, $g_{21}^2 = 2$, $\delta_{21}^2 = -511.228$, $g_{21}^1 = 100$, $\delta_{21}^1 = -600$, $C_{\mathrm{R}}^{12} = 600$), $|\delta_{21}^2| \neq C_{\mathrm{R}}^{12}$ accounts for the dynamical Stark-splitting.

3.2 Switching between local states

We now return to the stochastic simulation of the interacting and driven 2-level-pair. The selectivity condition is taken to apply approximately. Each system is in resonance if the neighbor system is in its respective ground state. The corresponding trajectories (for $g_{21}^1 \gg g_{21}^2$; $W_{12}^1 > 0$, $W_{12}^2 = 0$) in terms of the local Bloch-vector for the subsystem 2 are shown in Figure 4. "Shelving" is seen to dominate over the smooth dynamics expected for unitary motion. The weakly driven, locally undamped subsystem 2 performs a kind of telegraph signal. This telegraph signal, in turn, functions as a "switch" for the strongly driven subsystem 1, the luminescence of which is also shown. The model is equivalent to the three-level system as studied, *e.g.* in [24] in terms of telegraph-signals. The effective transition rates between "light" and "dark" have been derived in [25].

Sampling over many stochastic trajectories, we finally obtain the marginal probability density $f(\lambda_2^2, \lambda_3^2, t)$, as introduced in Section 2 (*cf.* [16]). Depending on the damping strength ("frequency of measurements"), this distribution is more or less peaked at the pertinent "shelving states" (see Fig. 5). These states deviate from the eigenstates $\lambda_3^1 = \mp 1$ ($\varphi = 0, \pi$), which are the attractor states for $g_{21}^2 = 0$ (as discussed in Sect. 2.6).

The peaked structure reflects the measurement-induced decomposition into two virtually separate Hilbert-space sections. For too weak damping this decomposition is not yet effective, *i.e.* the trajectories are not yet Zenon-trajectories proper.

A similar analysis of $f(\Gamma)$ could be carried out also for the following, more complicated scenarios. There is, as a function of parameters, a continuous transition between general trajectories and (approximate) Zenon-trajectories.

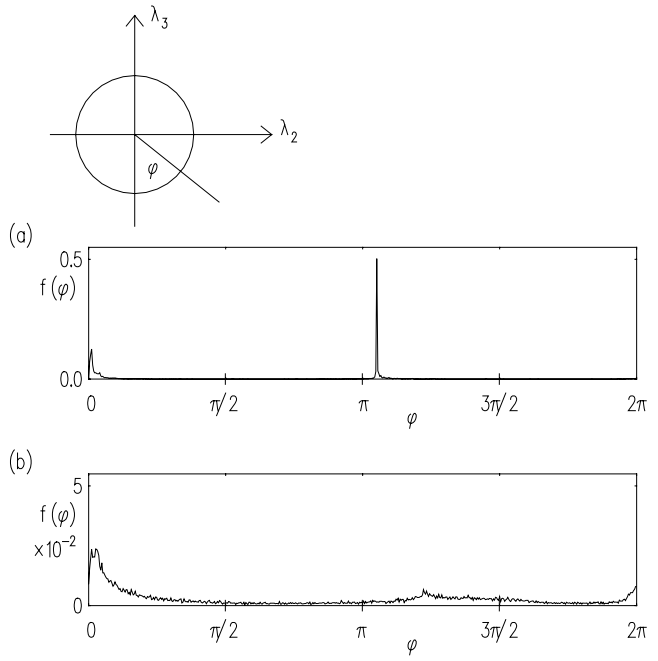

Fig. 5. Marginal probability density $f(\lambda_2^2, \lambda_3^2)$ of driven pair of damped two-level systems as of Figure 4. Inset shows definition of polar angle. (a) $W_{12}^1 = 70$, (b) $W_{12}^1 = 7$.

3.3 Switching between dynamical modes

We extend the model considered in Section 3.2 (see Fig. 4): the flipping system 2 (controlled by system 1) now controls the dynamics of a third system (Fig. 6). Detuning and coupling is chosen such that the third system now flips between a Rabi-oscillation and the fixed ground state, *i.e.* between two different dynamical modes. The two measurement outcomes, "dark" and "light", are connected here with different product state spaces of subsystem 2

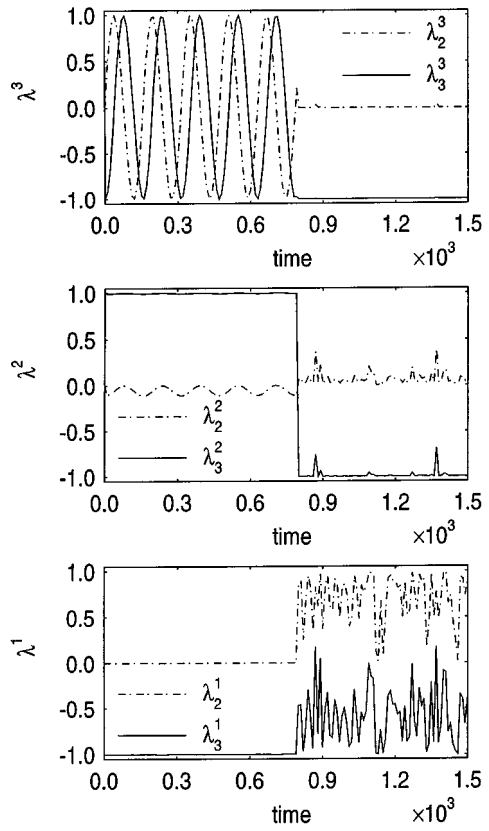

Fig. 6. Switching between ground state and Rabi-oscillations of system 3, coupled *via* system 2 to damped system 1. ($\lambda_1^\mu = 0$ and not shown.) Entanglement can be neglegted and is not shown here. Parameters are $W_{12}^1 = 1$, $g_{21}^1 = 0.6$, $\delta_{21}^1 = 40$, $g_{21}^2 = 0.02$, $\delta_{21}^2 = 0$, $g_{21}^3 = 0.04$, $\delta_{21}^3 = 40$, $C_{\rm R}^{12} = -C_{\rm R}^{23} = 40$.

and 3: contrary to the example of Section 3.4 entanglement can be neglected. This kind of "remote control" could be extended to even larger chains probed at one end.

3.4 Switching between Bell-states

Finally, Figure 7 shows the simulation of a $N = 3$ network under different conditions: system 1, which is damped and thus serves as the luminescence source, is sandwiched between the other subsystems, which are driven into slightly different Rabi-oscillations (see Eq. (29); $g_{21}^2 = 0.62$, $g_{21}^3 = 0.58$). Initially all 3 subsystems are in spin-down state ($\lambda_3^\mu = -1$). Detuning ($\delta_{21}^2 = \delta_{21}^3$), and coupling ($C_{\rm R}^{21} = C_{\rm R}^{31}$) are chosen in such a way that system 1 is in resonance, when the states of the neighbors are different (product states $|1(2)2(3)\rangle$, $|2(2)1(3)\rangle$) and off-resonant otherwise. (Note that system 1 can neither distinguish between $|1(2)2(3)\rangle$ and $|2(2)1(3)\rangle$, nor between $|1(2)1(3)\rangle$ and $|2(2)2(3)\rangle$; here the subsystem index is given in parenthesis.) System 2 and 3 are in resonance, if system 1 is in the ground-state $|1\rangle$. This "logic" leads, initially, to an "entrainment" of system 2 and 3, *i.e.* despite different Rabi-frequencies they remain in phase. Then, after deterministic "relaxation" into an highly entangled state, the

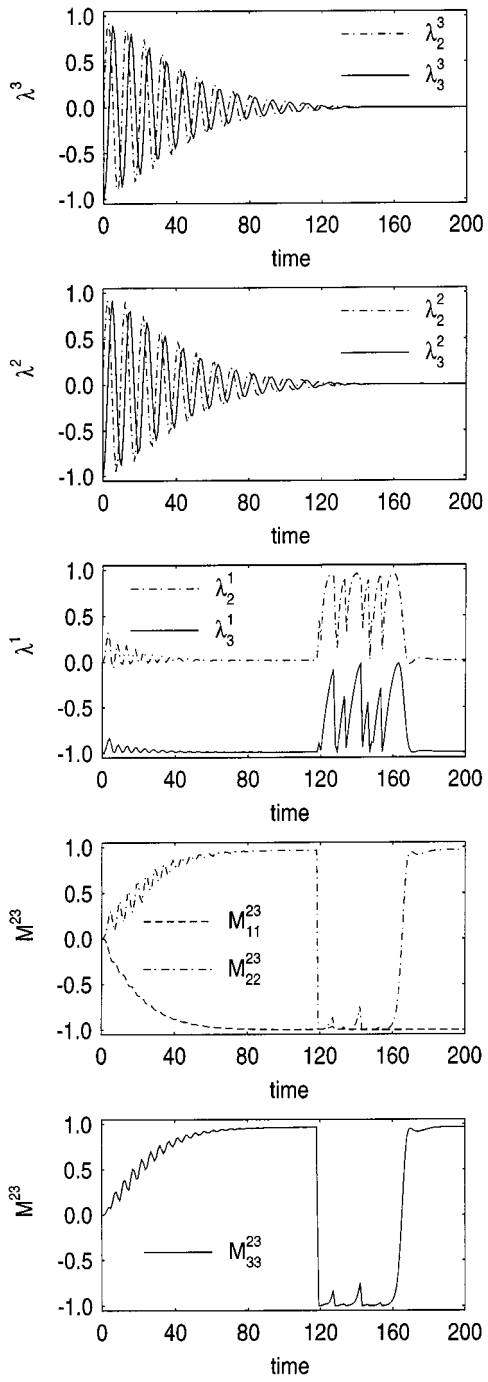

Fig. 7. Relaxation and switching between Bell-states of system 2 and 3 as induced by coupling to damped system 1. Parameters are $W_{12}^1 = 1$, $g_{21}^1 = 0.6$, $\delta_{21}^1 = 0$, $g_{21}^2 = 0.62$, $g_{21}^3 = 0.58$, $\delta_{21}^2 = \delta_{21}^3 = 40$, $C_{\rm R}^{12} = C_{\rm R}^{13} = -40$.

pair (2,3) switches roughly between Bell-state [26] $M_{ii}^{23} = -1$, $i = 1, 2, 3$ (*i.e.* $|\psi\rangle = \frac{1}{\sqrt{2}}[|12\rangle - |21\rangle]$) and Bell-state $M_{11}^{23} = -1$, $M_{22}^{23} = M_{33}^{23} = +1$ ($|\psi\rangle = \frac{1}{\sqrt{2}}[|11\rangle - |22\rangle]$). Due to the built-in logic, these two Bell-states are now associated with the two alternative measurement-outcomes, "light", "dark".

4 Closed networks: pulsed dynamics

In the Schrödinger picture the dynamics is carried by the time-dependent density operator. However, the $SU(2)$-parameters specifying the unitary dynamics need not be constant in time either: their time-dependence will have to be controlled externally. We consider 1-particle interactions $\Omega_{il}^{\mu\mu}$ (see Append. B),which can be changed simply by changing the parameters of the optical driving field. 2-particle terms ($Q_{ijk}^{\mu\mu\nu}$) may be modified by changing the spatial structure (distance or orientation of the subsystems) or by additional gates. In the examples considered here, these Hamiltonian $SU(2)$-parameters are taken to be piecewise constant in time. Pulsed dynamics is meant to refer to a situation, in which any of the parameters undergoes a rectangular pulse-shaped variation. We will show that under certain conditions individual subsystems, conditioned by other subsystems, may appear to emulate ensemble behavior.

4.1 Conditioning in closed system

Light pulses play an important role in the preparation of coherent states in atomic spectroscopy. For a rectangular pulse of duration Δt and center frequency ω_{ij} one defines $g_{ij}^{\mu}\Delta t = \pi$ ($\pi/2$) as a π ($\pi/2$)-pulse. The effect of the pulse, to be sure, also depends on the detuning. We will assume $\delta_{ij}^{\mu} = 0$ for all nodes μ not coupled to an optical driving field, and δ_{ij}^{μ} to remain constant as specified during the pulse acting on μ.

This type of coherent dynamics can be generalized to the interacting pair as discussed in Section 2.5: a π-pulse, $g_{21}^{1}\Delta t = \pi$, with $\delta_{21}^{1} = -C_{\mathrm{R}}^{12}$ and under the selectivity condition will invert Bloch-vector λ^1 only, if control 2 is in the ground state $\lambda^2 = (0, 0, -1)$; if it was in the excited state, the effective detuning would make the pulse ineffective. These two alternative paths constitute an implementation of the classical "controlled NOT" logic.

If the conditioning system 2 is in a local coherent state, *i.e.* in a superposition of the spin-up- and the spin-down-state [27], correlation builds up, as then $X_{ij} \neq 0$ (see Eq. (24)). The dynamics of subsystem 1, $\lambda_j^1(t)$, can be interpreted as the weighted average over the trajectories under resonant and off-resonant conditions, respectively, both starting from the same initial state ("quantum controlled NOT", [27,28]). This means that in this parameter window the *state probabilities* of subsystem 2 can be interpreted as the *path probabilities* (for switching and non-switching) of subsystem 1. Note that the network as a whole is always on a deterministic trajectory. No information gain is involved.

4.2 "Reversible projection"

We consider again the undamped two-node system as treated in Section 4.1, but now from the point of view of system 2, the control. For reasons that will become clear below, we will denote subsystem 1 as "memory".

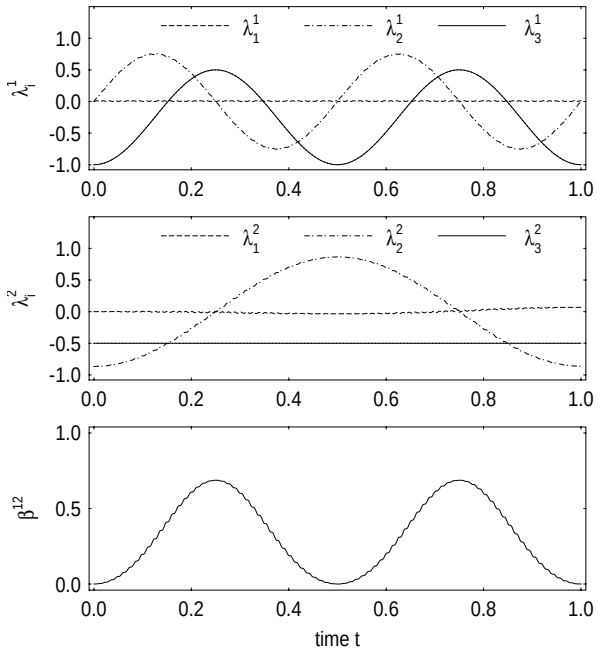

Fig. 8. Period doubling in an interacting network (N=2). Time in arbitrary units τ. Shown are the Bloch-vectors λ_j^{μ} and the entanglement measure β^{12}. $C_{\mathrm{R}}^{12} = -\delta_{21}^{1} = -\delta_{21}^{2} = 500$, $g_{21}^{1} = 4\pi$. Initial state: $\lambda_3^1 = -1$, $\lambda_1^2 = 0$, $\lambda_2^2 = -\sqrt{0.75}$, $\lambda_3^2 = -0.5$.

We momentarily assume $g_{21}^{2} = 0$, and see from equation (25) that λ_3^2 is a constant of motion. A typical trajectory generated by these equations is shown in Figure 8 for $|g_{21}^{1}| \ll |2C_{\mathrm{R}}^{12}|$ and the initial state $\lambda_3^1(0) = -1$ and $\lambda_j^2(0) = (0, -\sqrt{0.75}, -0.5)$. After completion of a nominal π-pulse, $g_{21}^{1}\Delta t = \pi, \delta_{\mathrm{eff}}^{1} = 0$, the network is found in an entangled state with $\lambda_1^1 = \lambda_2^1 = 0$ (local coherence removed) and β^{12} at its peak value. This again happens for $g_{21}^{1}\Delta t = 3\pi$. The period is $T^* = 4\pi/g_{21}^{1} = 2T$, where T would be the period of the Rabi-oscillation in the isolated subsystem 1.

For $|g_{21}^{1}| \gg |2C_{\mathrm{R}}^{12}|$ and the same initial conditions the effect of the inter-node coupling can be neglected: the dynamics of subsystem 1 becomes periodic with period T. In between no strict periodic behavior survives.

It is remarkable that the π-pulse on subsystem 1 has the effect of (reversibly) "projecting" system 2 on the measurement basis of the generator $\hat{\lambda}_3(2)$: this is exactly what one would expect from an ensemble-measurement based on the von Neumann projections

$$\lambda_j^2 \to (\lambda_j^2)' = (0, 0, \lambda_3') \tag{45}$$

where $\lambda_3' = m = \mp 1$ with probability $P_{\mp}^2 = 1/2(1 \mp \lambda_3^2)$. The ensemble average is $\overline{(\lambda_3^2)'} = \lambda_3^2$. The dynamics of the total network is such that system 2 behaves as if it represented this ensemble result. Of course, there is still a decisive difference to an actual measurement: no decision between "up" and "down" has been reached, and the removal of local coherence, $\lambda_{1,2}^2 = 0$, can still be undone, thanks to the non-local correlations (entanglements) present in the total system.

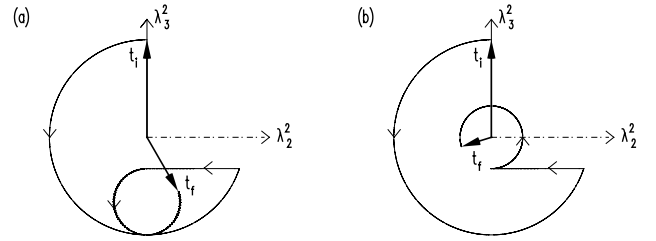

Fig. 9. "Reversible projection" in closed network (N=2): ($g_{21}^1 = 0$, $g_{21}^2 = 2\pi$), except during a π-pulse on subsystem $\mu = 1$ ($g_{21}^1 = 2\pi$, $g_{21}^2 = 0$). Shown is the back-action on object system $\mu = 2$ between time t_i and t_f for (a) $C_\mathrm{R}^{12} = -\delta_{21}^1 = -\delta_{21}^2 = 500$ constant, (b) $C_\mathrm{R}^{12} = -\delta_{21}^1 = -\delta_{21}^2 = 500$ during pulse only, zero otherwise.

4.3 Time windows

This concept of pulsed reversible projections can be generalized to an object system 2, which is subject to its own dynamics, *i.e.* we now let $g_{21}^2 > 0$ and constant, $g_{21}^1 = 0$, while $g_{21}^1 > 0$, $g_{21}^2 = 0$ during pulse duration. If $2|C_\mathrm{R}^{12}| \gg g_{21}^1, g_{21}^2$ we may choose the external frequency to be in resonance with the transition in subsystem 2 provided memory system 1 is in state $\lambda_3^1 = -1$, *i.e.* $\delta_{21}^2 = -C_\mathrm{R}^{12}$. If at some later time t_1 a π-pulse is applied to 1, the state of 1 may change and thus possibly push system 2 out of resonance. This situation is shown in Figure 9a: after "projection" the Bloch-vector of the object continues to rotate with the original Rabi-frequency, but with a reduced Bloch-vector length and a "down-shifted" center of rotation: projection at a time when $\lambda_3^2 = -1$ would make system 2 stop.

This dynamical back-action can be avoided if we make use of the fact that C_R (typically due to dipole-dipole interactions) sensitively depends on distance between the two subsystems or else may be controlled by additional gates. For the present purpose we will therefore assume that $C_\mathrm{R}^{12} = 0$ except during the short π-pulse: the resulting dynamics is shown in Figure 9b. During the pulse the two subsystems 1 and 2 become entangled and the Bloch-vector λ^2 is "projected" onto the 3-axis. Then, λ^2 continues to rotate with its original Rabi-frequency and its original center, but with the reduced length obtained by the projection.

Again, this is the behavior one would expect for an *ensemble* of driven two-level systems after an actual $\hat{\lambda}_3(2)$-measurement at time t_1, which would give the eigenvalue $m = \pm 1$ with the conditional probability

$$p(t_1, m \,|\, t_0, -1) = \frac{1}{2}\left(1 - m\cos\left[g_{21}^2(t_1 - t_0)\right]\right). \qquad (46)$$

After "projection", the individual object system 2 is thus in the same state as the actually measured ensemble,

$$\bar{\lambda}_3(t_1) = \cos\left[g_{21}^2(t_1 - t_0)\right]. \qquad (47)$$

As a consequence, for $t = t_0 + \Delta t > t_1$, where $g_{21}^1 \Delta t = \pi$, the probability to still find $m = -1$, has been increased from zero, the value without intermediate projection ("Zenon effect"). In the present case, however, thanks to the nonlocal information contained in M_{ij}^{12}, this projection can still be undone: applying a "negative" π-pulse just when the Bloch-vector has returned to the position at the time of its original projection, the vector resumes its original rotation with $|\lambda^2| = 1$ (alternatively we may apply a 3π-pulse, *cf.* Fig. 8).

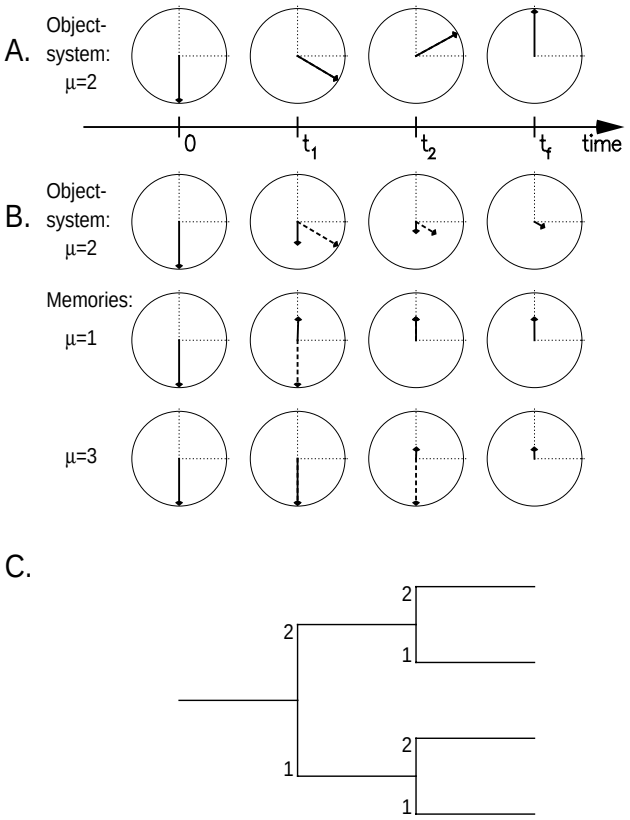

Fig. 10. Sequence of "reversible projections" in a closed network (N=3). Object system $\mu = 2$ continuously driven ($g_{21}^2 = \pi$, $\delta_{21}^2 = 0$). Memory system $\mu = 1\,(3)$ is subject to selective π-pulse at time $t_1\,(t_2)$ during which $C_\mathrm{R}^{12} = -\delta_{21}^1 = -\delta_{21}^2 = 500$ ($C_\mathrm{R}^{23} = -\delta_{21}^2 = -\delta_{21}^3 = 500$). Initial state of all 2-level systems is $\lambda_3^\mu = -1$. Shown are the Bloch-vectors in λ_2/λ_3-plane. A) bloch-vector of isolated object system, B) full network as described above. Broken (solid) arrows: state before (after) respective π-pulse, C) decision tree: single object-system realizes all possible paths through states 1,2 in parallel.

4.4 Mixture of trajectories

We now consider a network consisting of an object system, a first memory $\mu = 1$, and a second memory $\mu = 3$. The equations of Section 2.5 apply with different initial conditions. In the simplest case with no dynamics of object system 2 ($g_{21}^2 = 0$), this would correspond to a repetition of the previous "projection" at a later time $t_2 > t_1$ (*i.e.* $K_{33}^{13} = 1$). However, we may now let the object 2 undergo a coherent dynamics of its own. The two memories will then see different object states. The corresponding numerical simulation is shown in Figure 10: (it is assumed

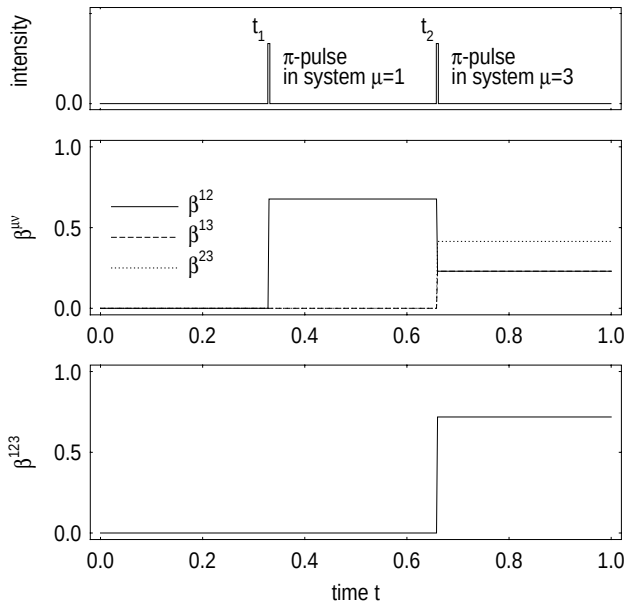

Fig. 11. Entanglement measures as defined in equations (12, 13), corresponding to Figure 10.

that $C_{\rm R}^{12}$, $C_{\rm R}^{23}$ are unequal zero during the respective test π-pulses only). The removal of local coherence in the object system is clearly seen. This closed (though explicitly time-dependent) three-node system makes subsystem 2 look as if an homogeneous ensemble of systems 2 were measured twice. The corresponding "decision tree" is also indicated, which is realized here by one single object system in parallel. The Zenon effect at time $t_{\rm f} = \pi/g_{21}^2 = T/2$ is clearly seen: the probability to find object 2 still in its initial state has further increased. We also note that the correlation between the memories is given by

$$K_{33}^{13} \approx \cos\bigl[g_{21}^2(t_2 - t_1)\bigr] \tag{48}$$

which would hold exactly for $g_{21}^2/2|C_{\rm R}^{\mu 2}| \to 0$. The right-hand site is the 2-time correlation function $\langle \hat{\lambda}_3^2(t_1)\, \hat{\lambda}_3^2(t_2)\rangle$ for a coherently driven object system 2 [29]: time is thus mapped onto subsystem-index space. The corresponding build-up of entanglement is shown in Figure 11 in terms of the entanglement measures (see Eqs. (12, 13)). Note that also the two memories have become entangled even though they have never directly interacted.

This scenario could be enlarged to include further memories and thus additional "projections". At fixed time $t_{\rm f}$ the local Bloch-vector (*i.e.* the reduced density matrix) of the object system would then more and more approach state $|1\rangle$. However, due to the finite duration of each pulse, we cannot pack infinitely many "projections" into a limited period of time: the probability to have left state $|1\rangle$ at time $t_{\rm f}$ thus remains finite.

In any case, these potential Zenon-trajectories are examples of the more general concept of "consistent histories" [30], which can be assigned classical probabilities.

4.5 Delayed measurements

The final entangled state of the network (as prepared according to Section 4.4 and shown in Figure 10) will now be measured. This can be done by means of measurement gates as discussed in Section 2.6, or, simpler, by means of a direct von Neumann projection. The measurement of the memory gates can be performed in any order. A specific sequence is shown in Figure 12: projection in object system 2 (at time $t_{\rm a}$), then projection in memory system $M2$ ($\mu = 3$). Due to the mapping of the time windows t_1, t_2 onto the index-space of supplementary memory subsystems (here $\mu = 1, 3$), this measurement sequence corresponds to a "travel backward in time": we first decide on the state of $\mu = 2$ "now" and then on its state at $t = t_2$. We note that each measurement readjusts the Bloch-vectors also of those systems not yet measured. This nonlocal effect derives from the entanglement of the network. It is thus guaranteed that the previous time decisions will not be inconsistent with the later decisions already established. The final measurement would be that of memory $M1$ ($\mu = 1$) establishing the state of the object at time $t = t_1$. In this way, the set of potential trajectories is turned into a single actual one.

4.6 Quantum parallelism

We note in passing that a closed system dynamics conditioned by pulsed parameter variations underlies also recent models of quantum computing (see *e.g.* [31]). For such a quantum computer to work one would need a conditioning such that a single subsystem of the network, while exploring all the ensemble properties, would finally end up with high probability in a state representing the desired solution, which was then measured (*cf.* Sect. 4.5). Additional Zenon effects have been proposed for some kind of error correction [32].

There are a number of arguments which may help to understand the expected computational efficiency: one may refer to the tremendously large Hilbert-space underlying general superposition states or to the power of interference in suppressing/enhancing certain states in a non-additive fashion. Another, and possibly more direct way is to realize that a single subsystem can emulate a whole ensemble. This "quantum parallelism" would obviously be the method of choice to save hardware, if there was not a severe constraint: the final measurement cannot be an ensemble measurement but rather a stochastic projection. The design of special quantum algorithms has to make sure that this projection, nevertheless, leads to useful results.

Recently, it has been proposed [33] to emulate, in turn, single quantum computers by appropriately prepared ensembles. These ensembles would then be made to emulate another ensemble, as required by the quantum algorithm. Whether any of these concepts can be realized on larger scale remains doubtful.

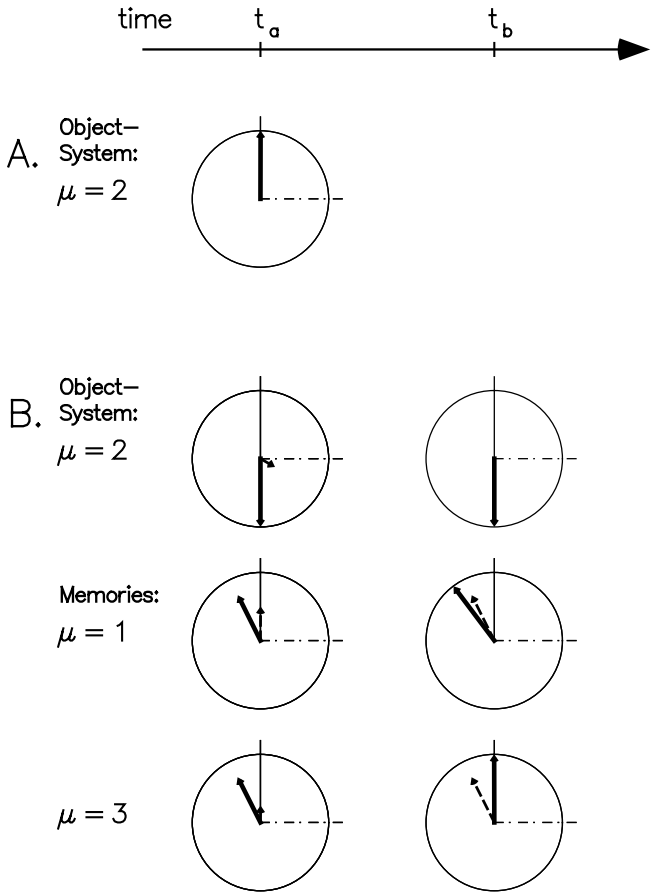

Fig. 12. Sequence of measurement projections on the $N = 3$ network as prepared according to Figure 10. t_a: projection in system $\mu = 2$, t_b: projection in memory system $\mu = 3$; A) state of object system (for comparism), B) full network. Broken (solid) arrows: state before (after) projection.

5 Summary and conclusions

Damping related with information retrieval modifies the dynamics of quantum system on the ensemble- and on the single-system level (trajectories). Quantum Zenon effects have been discussed here in terms of special classes of such quantum trajectories. These trajectories are special in the sense that they (i) require appropriate parameter windows (establishing the "logic of inference"), (ii) are associated with "continuous" alternative measurement signals (here: "light"/"dark"), (iii) are constrained to disjoint subspaces labelled by those measurement outcomes, and (iv) occasionally jump between the subspaces on a time-scale large compared with the reciprocal rate of the damping channel (see Fig. 13). This conditioned behaviour will typically show up also in the (stationary) distribution function of the state parameters, which will be peaked as a function of the "distinguishing" parameter subset.

We note that those features deviate from what might be called the "idealized Zenon effect": (a) there is no complete freeze-in (as the number of measurements per given time cannot become infinite), (b) the conditioning will, in general, not lead to fixed "points" in state-space, but

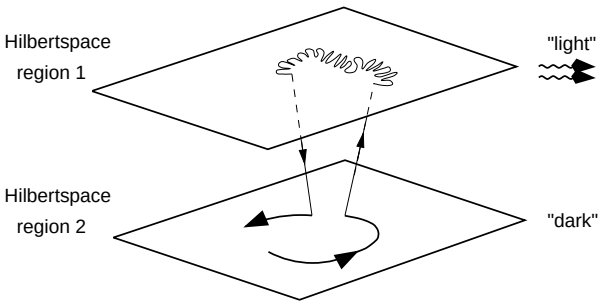

Fig. 13. Zenon-trajectory: the quantum trajectory is conditioned by 2 different measurement outcomes, between which there are occasional jumps. Light emission leads to a residual "Zitterbewegung".

rather — in particular for composite systems — to disjoint extended subspaces, and (c), because of the residual non-deterministic jump dynamics resulting from (a), the Zenon-features tend to become washed out in the ensemble limit.

Nevertheless, ensemble Zenon effects, being the main focus of virtually all previous work, survive on a small time-scale and for a coherent initial ensemble state. Ironically, however, this short-time Zenon effect is not a "watchdog" effect at all, *i.e.* it does not require actual information retrieval. Closed composite systems (with pulsed interactions) can emulate this behaviour with respect to a subsystem.

Similar conclusions have been reached in [13], though in the ensemble limit and without explicit model. Reference [14] proposes a sequence of Stern-Gerlach-type filtering to suppress the spin-motion induced by an homogeneous magnetic field.

In a more general sense one main theme underlying the Quantum Zenon effect is stabilization. This is also at the heart of quantum computing, which aims to exploit quantum parallelism.

In continuous measurements the observables tend to become available almost at any time, like for a classical object. Typical luminescence records consist of "light" and "dark" periods ("1-bit-channel").

In the dark periods "nothing happens" (zero measurement). In general, the conditioned system dynamics may then deterministically involve an oscillatory behavior or a relaxation to a fixed state, depending on the system parameters. We have shown that this can be analyzed in terms of complex dressed states.

The light periods are characterized by a dense sequence of projections in the damped subsystem 1, which virtually freezes its ground state; this, in turn, conditions the dynamics of the other interacting subsystems, depending on the "logic of inference".

The present model containing one output channel (single binary decisions) can and must be generalized to multiple channels. However, this does not change the principle nature of how quantum systems navigate between the concepts of "change" and persistent "properties".

Quantum Zenon effects are neither paradoxical nor do they require special experimental efforts to show up. The theoretical and experimental study of Zenon-trajectories, though, should still contribute to a better understanding of the various classes of trajectories that may exist in nature.

We thank J. Schlienz for valuable discussions, and the Deutsche Forschungsgemeinschaft for financial support.

Appendix A: $SU(2)$-generators

In two-dimensional Hilbert-space spanned by the states $|1\rangle$, $|2\rangle$ we define the transition-operators

$$\hat{P}_{ij} = |i\rangle\langle j| \,, \quad i,j = 1,2. \tag{A.1}$$

The $SU(2)$-generators are then taken to be (Pauli-matrices)

$$\begin{aligned} \hat{\lambda}_1 &= \hat{P}_{12} + \hat{P}_{21} \\ \hat{\lambda}_2 &= I(\hat{P}_{12} - \hat{P}_{21}) \\ \hat{\lambda}_3 &= \hat{P}_{22} - \hat{P}_{11}. \end{aligned} \tag{A.2}$$

Pertinent properties are

$$\mathrm{Tr}\,\{\hat{\lambda}_i\,\hat{\lambda}_j\} = 2\delta_{ij} \tag{A.3}$$

$$\mathrm{Tr}\,\{\hat{\lambda}_i\} = 0 \tag{A.4}$$

$$\hat{\lambda}_i\,\hat{\lambda}_j = -\hat{\lambda}_j\,\hat{\lambda}_i \quad (i \neq j) \tag{A.5}$$

$$\left[\hat{\lambda}_i,\,\hat{\lambda}_j\right] = 2\,I\,\varepsilon_{ijk}\hat{\lambda}_k \tag{A.6}$$

where ε_{ijk} is the totally antisymmetric tensor.

Appendix B: Representation of the Lindblad operator

The Lindblad master equation reads

$$\frac{\mathrm{d}}{\mathrm{dt}}\hat{\rho} = \hat{L}^{(0)}\hat{\rho} + \hat{L}^{(H)}\hat{\rho} + \hat{L}^{(P)}\hat{\rho}. \tag{B.1}$$

Taking the trace of this equation with the operators $\hat{\lambda}_i(\mu)$, $\hat{K}_{ij}(\mu\nu)$ *etc.* one gets the time-derivative of the respective expectation values, $\frac{\mathrm{d}}{\mathrm{dt}}\lambda_i^\mu$, $\frac{\mathrm{d}}{\mathrm{dt}}K_{ij}^{\mu\nu}$ *etc.* For a local Hamiltonian coupling acting on subsystem 1, for example, one finds for the rhs:

$$\mathrm{Tr}\left\{\left(\hat{L}^{(0)}\hat{\rho}\right)\hat{\lambda}_i(1)\right\} = \Omega_{ik}^{11}\lambda_k^1 \tag{B.2}$$

$$\mathrm{Tr}\left\{\left(\hat{L}^{(0)}\hat{\rho}\right)\hat{K}_{ij}(1\mu)\right\} = \Omega_{il}^{11}K_{lj}^{1\mu} \tag{B.3}$$

$$\mathrm{Tr}\left\{\left(\hat{L}^{(0)}\hat{\rho}\right)\hat{K}_{ijk}(123)\right\} = \Omega_{im}^{11}K_{mjk}^{123} \tag{B.4}$$

where

$$\Omega_{ik}^{\mu\mu} = \frac{1}{4\hbar}\varepsilon_{ijk}H_j^\mu. \tag{B.5}$$

For the Hamilton-parameters given in (6) one readily gets

$$\begin{aligned} \Omega_{12}^{11} &= -\Omega_{21}^{11} = -\delta_{21}^1 \\ \Omega_{23}^{11} &= -\Omega_{32}^{11} = -g_{21}^1. \end{aligned} \tag{B.6}$$

(All other parameters are zero.) For a bilocal coupling between node $\mu = 1$ and $\mu = 2$ the result is

$$\begin{aligned} \mathrm{Tr}\left\{\left(\hat{L}^{(0)}\hat{\rho}\right)\hat{\lambda}_i(1)\right\} &= \frac{1}{2}Q_{ikl}^{112}K_{kl}^{12} \\ \mathrm{Tr}\left\{\left(\hat{L}^{(0)}\hat{\rho}\right)\hat{\lambda}_i(2)\right\} &= \frac{1}{2}Q_{ikl}^{212}K_{kl}^{12} \\ \mathrm{Tr}\left\{\left(\hat{L}^{(0)}\hat{\rho}\right)\hat{K}_{ij}(12)\right\} &= \frac{1}{2}Q_{ijl}^{121}\lambda_l^1 + \frac{1}{2}Q_{ijl}^{122}\lambda_l^2 \\ \mathrm{Tr}\left\{\left(\hat{L}^{(0)}\hat{\rho}\right)\hat{K}_{ik}(13)\right\} &= \frac{1}{2}Q_{iml}^{112}K_{mlk}^{123} \\ \mathrm{Tr}\left\{\left(\hat{L}^{(0)}\hat{\rho}\right)\hat{K}_{jk}(23)\right\} &= \frac{1}{2}Q_{jml}^{112}K_{mlk}^{123} \\ \mathrm{Tr}\left\{\left(\hat{L}^{(0)}\hat{\rho}\right)\hat{K}_{ijk}(123)\right\} &= \frac{1}{2}Q_{ijl}^{121}K_{lk}^{13} + \frac{1}{2}Q_{ijl}^{122}K_{lk}^{23} \end{aligned} \tag{B.7}$$

where

$$Q_{ijk}^{\mu\mu\nu} = \frac{1}{2\hbar}\varepsilon_{ilj}H_{lk}^{\mu\nu}. \tag{B.8}$$

The Hamilton-model, (Eq. (7)), leads to [16,17]

$$\begin{aligned} Q_{231}^{212} &= -Q_{132}^{212} = 2\,C_{\mathrm{R}}^{12} \\ Q_{123}^{112} &= -Q_{213}^{112} = 2\,C_{\mathrm{R}}^{12}. \end{aligned} \tag{B.9}$$

For a local damping channel in node $\mu = 1$

$$\begin{aligned} \hat{F}(1) &= \sqrt{2}\,\hat{P}_{12}(1) \\ \hat{F}^+(1) &= \sqrt{2}\,\hat{P}_{21}(1) \end{aligned} \tag{B.10}$$

one has ($\mu \neq 1$)

$$\begin{aligned} \mathrm{Tr}\left\{\left(\hat{L}^{(H)}\hat{\rho}\right)\hat{\lambda}_i(1)\right\} &= -\frac{W_{12}^1}{2}\left(\delta_{i3} + \lambda_i^1\right) \\ \mathrm{Tr}\left\{\left(\hat{L}^{(H)}\hat{\rho}\right)\hat{K}_{ij}(1\mu)\right\} &= -\frac{W_{12}^1}{2}\left(\delta_{i3}\lambda_i^\mu + K_{ij}^{1\mu}\right) \\ \mathrm{Tr}\left\{\left(\hat{L}^{(H)}\hat{\rho}\right)\hat{K}_{ijk}(123)\right\} &= -\frac{W_{12}^1}{2}\left(\delta_{i3}K_{jk}^{23} + K_{ijk}^{123}\right) \end{aligned} \tag{B.11}$$

and

$$\begin{aligned} \mathrm{Tr}\left\{\left(\hat{L}^{(P)}\hat{\rho}\right)\hat{\lambda}_3(1)\right\} &= -\frac{W_{12}^1}{2}\left(1 + \lambda_3^1\right) \\ \mathrm{Tr}\left\{\left(\hat{L}^{(P)}\hat{\rho}\right)\hat{K}_{3j}(1\mu)\right\} &= -\frac{W_{12}^1}{2}\left(\lambda_j^\mu + K_{3j}^{1\mu}\right) \\ \mathrm{Tr}\left\{\left(\hat{L}^{(P)}\hat{\rho}\right)\hat{K}_{3jk}(123)\right\} &= -\frac{W_{12}^1}{2}\left(K_{jm}^{23} + K_{3jk}^{123}\right) \end{aligned} \tag{B.12}$$

while $(\mu,\nu \neq 1)$

$$\begin{aligned}
\mathrm{Tr}\left\{\left(\hat{L}^{(H)}\hat{\rho}\right)\hat{\lambda}_j(1)\right\} &= -\mathrm{Tr}\left\{\left(\hat{L}^{(P)}\hat{\rho}\right)\hat{\lambda}_j(1)\right\} \\
&= -\frac{W_{12}^1}{2}\left(\lambda_j^\mu + K_{j3}^{\mu 1}\right) \\
\mathrm{Tr}\left\{\left(\hat{L}^{(H)}\hat{\rho}\right)\hat{K}_{jk}(\mu\nu)\right\} &= -\mathrm{Tr}\left\{\left(\hat{L}^{(P)}\hat{\rho}\right)\hat{K}_{jk}(\mu\nu)\right\} \\
&= -\frac{W_{12}^1}{2}\left(K_{jk}^{\mu\nu} + K_{jk3}^{\mu\nu 1}\right) \\
\mathrm{Tr}\left\{\left(\hat{L}^{(H)}\hat{\rho}\right)\right\} &= -\mathrm{Tr}\left\{\left(\hat{L}^{(P)}\hat{\rho}\right)\right\} \\
&= -\frac{W_{12}^1}{2}\left(1+\lambda_3^1\right). \qquad \text{(B.13)}
\end{aligned}$$

We see that the damping in subsystem 1 has non-local effects also on expectation-values not involving index 1. However, when added, the last set of equations (B.13) cancels, while the others give

$$\begin{aligned}
\mathrm{Tr}\left\{\left(\hat{L}^{(H)}\hat{\rho}+\hat{L}^{(P)}\hat{\rho}\right)\hat{\lambda}_i(1)\right\} &= \eta_i^1 + \xi_{ik}^{11}\lambda_k^1 \\
\mathrm{Tr}\left\{\left(\hat{L}^{(H)}\hat{\rho}+\hat{L}^{(P)}\hat{\rho}\right)\hat{K}_{ij}(1\mu)\right\} &= \eta_i^1\lambda_j^\mu + \xi_{il}^{11}K_{lj}^{1\mu} \\
\mathrm{Tr}\left\{\left(\hat{L}^{(H)}\hat{\rho}+\hat{L}^{(P)}\hat{\rho}\right)\hat{K}_{ijk}(123)\right\} &= \eta_i^1 K_{jk}^{23} + \xi_{im}^{11}K_{mjk}^{123} \qquad \text{(B.14)}
\end{aligned}$$

with

$$\begin{aligned}
\eta_i^1 &= -W_{12}^1\,\delta_{i3} \\
\xi_{11}^1 = \xi_{22}^1 &= -\frac{1}{2}W_{12}^1 \\
\xi_{33}^1 &= -W_{12}^1. \qquad \text{(B.15)}
\end{aligned}$$

References

1. The position measurement of a particle in a double-well potential is somewhat inbetween, see M.J. Gagen, H.M. Wiseman, G.J. Milburn, Phys. Rev. A **48**, 132 (1993).
2. B. Misra, E.C.G.Sudershan, J. Math. Phys. **18**, 756 (1977).
3. P. Knight, Nature **344**, 493 (1990).
4. E. Joos, Phys. Rev. D **29**, 1626 (1984).
5. J. von Neumann, *Mathematical Foundations of Quantum Mechanics*, Princeton U.P., 1955.
6. W.M. Itano, D.J. Heinzen, J.J. Bollinger, D.J. Wineland, Phys. Rev. A **41**, 2295 (1990).
7. For a recent proposal relating to the Zenon effect see: P. Kwiat, H. Weinfurter, A. Zeilinger, Sci. American **275**, 52 (1996).
8. S. Inagaki, M. Namiki, T. Tajiri, Phys. Lett. A **166**, 13 (1992).
9. T. Petrosky, S. Tasaki, I. Prigogine, Phys. Lett. A **151**, 109 (1990).
10. L.E. Ballentine, Phys. Rev. A **43**, 5165 (1991).
11. A. Beige, G.C.Hegerfeld, Phys. Rev. A **53**, 53 (1996).
12. W.L. Power, P.L. Knight, Phys. Rev. A **53**, 1052 (1996).
13. D. Home, M.A.B. Whitaker, Phys. Lett. A **173**, 327 (1993).
14. S. Pascazjo, M. Namiki, Phys. Rev. A **50**, 4582 (1994).
15. V. Frerichs, A. Schenzle, Phys. Rev. A **44**, 1962 (1991).
16. G. Mahler, K. Keller, R. Wawer, Z. Phys. B **104**, 153 (1997).
17. M. Keller, G. Mahler, J. mod. Optics **41**, 2537 (1994).
18. K. Molmer, Y. Castin, J. Dalibard, J. Opt. Soc. Am. B **10**, 524 (1993).
19. A. Peres, A. Ron, Phys. Rev. A **42**, 5720 (1990).
20. C. Chu, W.P. Reinhardt, Phys. Rev. Lett. **39**, 1195 (1977).
21. A. Maque, S. Chu, W.P. Reinhardt, Phys. Rev. A **27**, 2946 (1983).
22. "Dark" states would be special complex dressed states witch zero imaginary part, see, *e.g.*, S.M. Chumakov, K.E. Hellwig, A.L. Rivera, Phys. Lett. A **197**, 73 (1995).
23. M. Ueda, M. Kitagawa, Phys. Rev. Lett. **68**, 3424 (1992).
24. Th. Sauter, W. Neuhauser, R. Blatt, P.E. Toschek, Phys. Ref. Lett. **57**, 1696 (1986).
25. H.J. Kimble, R.J. Cook, A.L. Wells, Phys. Rev. A **34**, 3190 (1986).
26. S.L. Braunstein, A. Mann, M. Revzen, Phys. Rev. Lett. **68**, 3259 (1992).
27. T. Sleator, H. Weinfurter, Phys. Rev. Lett. **74**, 4087 (1995).
28. G. Mahler, V.A. Weberruß, *Quantum Networks: Dynamics of Open Nanostructures* (Springer, Berlin, New York, 1995).
29. J.P. Paz, G. Mahler, Phys. Rev. Lett. **71**, 3235 (1993).
30. R. Omnés, Rev. mod. Phys. **64**, 339 (1992).
31. D.P. Di Vincenco, Science **270**, 255 (1995).
32. A. Berthiaume, D. Deutsch, R. Jozsa, in *Proceeding of Workshop on Physics and Computation – PhysComp 94* (IEEE Computer Society Press, Dallas 1994).
33. N.A. Gershenfield, I.L.Chuang, Science 1997 (in press).